Supplementary

DLS measurement of the size of reverse micelles

We used dynamic light scattering (DLS, DynaPro NanoStar, Wyatt Technology) to measure the size of the reverse micelles. Because of the color interference from OX063 trityl, we prepared a DLS sample that was identical to the one used in our DNP-NMR experiments but without OX063 trityl. We estimated that the viscosity of a mixture of isooctane and 2-butanol in a 7:3 volume ratio is very close to that of water,[1] enabling us to use the default value for the required solvent viscosity setting. The data were automatically processed in the machine. The results (**Fig. S1**) reveal that the majority of the reverse micelles have a diameter of 14.2 nm, or a radius of 7.1 nm.

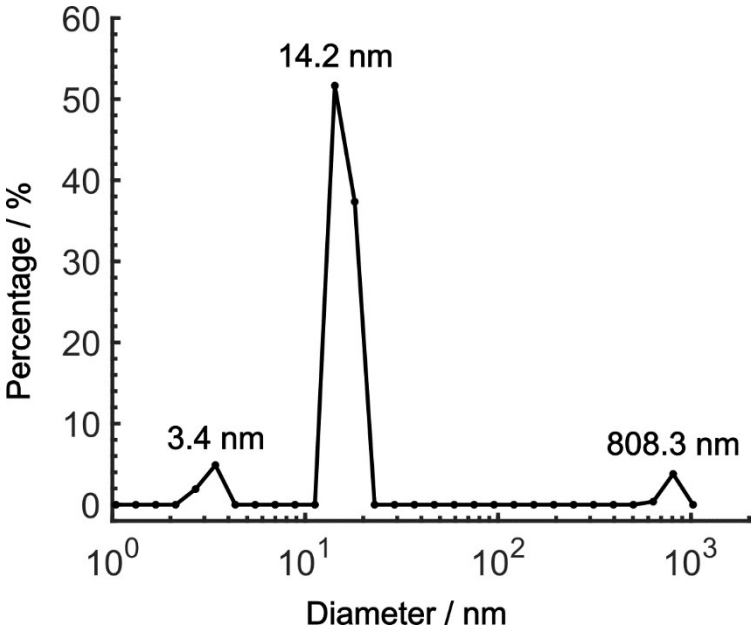

Fig. S1 The DLS results for the reverse micelles. The curve shows the percentage distribution of the diameters of the reverse micelles. The diameters corresponding to each peak of the distribution are indicated in the figure.

ESR checking of the potential leakage of OX063 trityl

We conducted electron-spin resonance (ESR) experiments to investigate the potential leakage of OX063 trityl. Given the weak mutual solubility between 2-butanol and water,[2] we were concerned that, if a small amount of water was present in the nonpolar phase of the reverse micelle system, the OX063 trityl might also exhibit weak solubility in that phase. To test this hypothesis, we acquired two ESR spectra using an X-band ESR spectrometer (BRUKER ELEXSYS-II E500 CW-EPR). The first spectrum was obtained from the sample used in our DNP-NMR experiments. For the second spectrum, we prepared a sample with identical components to the first but without AOT. This preparation resulted in phase separation, yielding a transparent supernatant and a lower phase in which a high concentration of OX063 trityl was visibly present. We then used the supernatant for the ESR measurement. The results are displayed in **Fig. S2**. The ESR spectrum of the sample

used in the DNP-NMR experiments showed a clear signal of OX063 trityl.[3,4] By contrast, the ESR spectrum of the supernatant from the sample without AOT showed no OX063 trityl signal. Therefore, we concluded that OX063 trityl did not leak from the reverse micelle into the nonpolar phase.

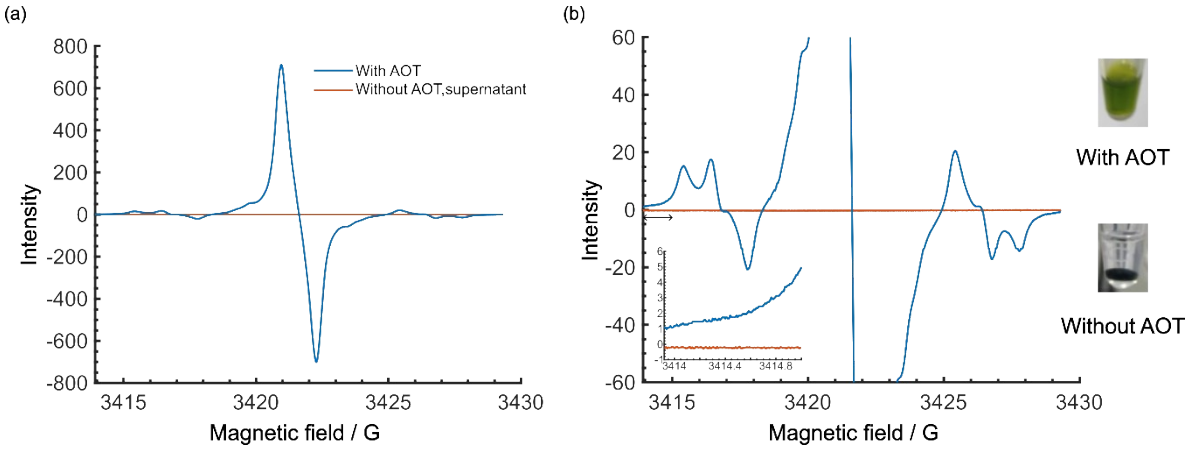

Fig. S2 The ESR spectra for evaluating OX063 trityl leakage. (a) The blue spectrum was acquired for the sample from the DNP-NMR experiments, whereas the orange spectrum was acquired for the supernatant of a sample identical to the first but without AOT. (b) A vertical blowup of (a). The features near the noise level seen in the blue data are the satellite peaks due to the hyperfine interaction with natural abundance ^{13}C.[4] The inset in (b) is further zooming in to the region from 3413.92 to 3415 G (indicated by a double arrow), showing the thermal noise level of the spectra. Photos of each sample are provided adjacent to the spectra.

DNP frequency profile of OX063 trityl

To determine the microwave frequencies for positive and negative DNP and to clarify the DNP mechanism for the observed DNP enhancement, we recorded the DNP frequency profile (**Fig. S3**). The data were acquired by scanning the microwave frequency around the electron resonance of OX063 trityl and recording the intensity of the main peak for ^{13}C-labeled urea. Because of the limited frequency range of our microwave source (a gyrotron), the negative enhancement peak is not fully captured in the profile. Nonetheless, the absolute value of the maximum negative enhancement is adequately close to that of the positive enhancement peak. On the basis of these results, we used 459.80 GHz for positive DNP and 460.19 GHz for negative DNP. This limitation in the microwave frequency range also restricts our focus to ^{13}C DNP experiments. We note that the frequency difference between the maximum positive and negative enhancement is approximately twice the ^{13}C Larmor frequency. Thus, we deduced that the primary DNP mechanism in our experiments is the solid effect. Given that the solid effect occurs in a two-spin system consisting of one electron spin and one nuclear spin, this result suggests that the majority of the reverse micelles contain no more than one OX063 trityl molecule.

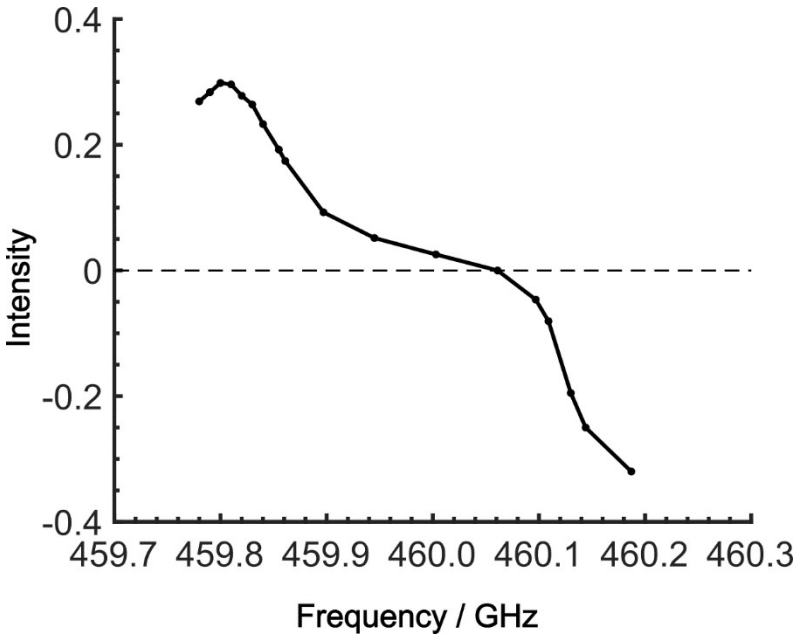

Fig. S3 The OX063 trityl-induced ^{13}C DNP frequency profile. The horizontal dashed line at $y = 0$ is included as a guide.

Model of DNP build-up and spin-diffusion

We built a model to analyze the polarization build-up process by fitting the experimental build-up curves. The analysis was conducted with **Equation (S1)**, a classic one-dimensional diffusion equation for the spin polarization $M(x,t)$ at a distance x from the PA and at time t:

$$\frac{\partial M(x,t)}{\partial t} = D_i \frac{\partial^2 M(x,t)}{\partial x^2} + R_{1,i}\left(M_{0,i} - M(x,t)\right) \quad \text{(S1)}$$

We considered a thin polarization source (S) region ($x = (0, x_S]$) directly hyperpolarized by the PA (at $x = 0$), surrounded by the target (T) region ($x = (x_S, x_T]$) and then the background (B) region ($x = (x_T, x_B]$). Accordingly, Equation S1 has location-dependent parameters: the spin-diffusion rate D_i, the longitudinal relaxation rate $R_{1,i}$, and the equilibrium polarization $M_{0,i}$, where $i \in$ [S, T, B] (**Fig. S4**).

In the source region, DNP drives the polarization toward $M_{0,S}$ for positive DNP conditions and toward $-M_{0,S}$ for negative DNP conditions with a rate $R_{1,S}$. The intrinsic spin relaxation rate here is absorbed into the DNP build-up process for simplicity. In the target and background regions, as well as in the source region when the MW source is off, the polarization relaxes toward the normalized thermal equilibrium value, $M_{0,S/T/B} = 1$, with the rate $R_{1,S} = R_{1,T}$ and $R_{1,B}$. The spin-diffusion rate in the T and B regions can be scaled to each other using the known ^{13}C density $\rho_{^{13}C}$ for each region and the relation $D \sim \rho_{^{13}C}^{1/3}$. For the reverse-micelle sample described in the main text, $D_B = 0.688 D_T$. The point $x = x_B$ was treated as the midpoint between two micelles.

The equation is numerically solved using initial condition $M(x,0) = 0$ and the Neumann boundary condition $\frac{\partial M(x,t)}{\partial t}|_{x = 0,\, x_B} = 0$. The parameters were optimized using a simulated annealing module in MATLAB (version R2023b, MathWorks, Natick, Massachusetts). The fitting results were stable in the sense that repetition using random initial values yielded similar optimized parameters. The simulated time–space distribution of the polarization was separately integrated for the T and B regions for fitting the target and background peak build-ups.

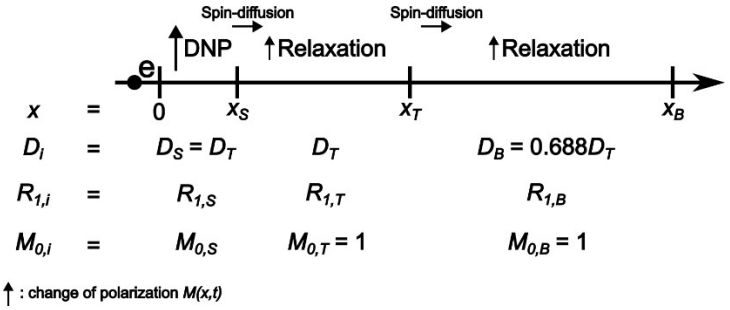

Fig. S4 One-dimensional diffusion model with the parameters that require optimization. Distances that partition the model into three regions are marked on the diagram. The location-dependent parameters corresponding to each of these regions are shown in the figure. The mechanisms by which the polarization changes are also indicated in the figure.

Method of simulation of contrast factor

Contrast factor build-up curves were simulated based on the polarization simulation described above. The simulated space–time dependence of the polarization at a given build-up time τ was integrated from 0 to x_T as the target signal intensity and integrated from x_T to x_B as the background signal intensity. The target and background signal intensities post-application of the MW-off subtraction and the Oops treatment, DNP(+) − DNP(off) and DNP(+) − DNP(-), were calculated. To align the simulation to experiments, the target signal intensity of the sample was further scaled by a constant $k_t = 0.90$, and the background signal intensity was scaled by $k_b = 0.71$. This scaling ensures that the calculated values at τ = 20,000 s after the application of DNP(+) − DNP(-) were equal to their corresponding experimental counterparts. The difference between the constants k_t and k_b can account for the experimental details not included in the model, such as the difference in the concentration of ^{13}C spins inside and outside the reverse micelles. After this process, the noise level in the simulation was designated as the experimental background signal intensity at τ = 0 s post-application of the Oops treatment. In the simulation of contrast factor with altered parameters, the noise level was kept the same for simplicity. Because the signal intensity for the experimental calculation of the contrast factor is the integral of the absolute value around the target or background peaks post-application of background signal suppression, the standard deviation of noise is derived as $\sigma = noise * \sqrt{(\pi/2)}$. To represent the effect in the simulation where very small signal intensities are elevated to the noise level while large signal intensities remain unaffected, the noise-adjusted signal intensity was calculated as $S_n = F(S,\sigma)$, where *F* is the

expectation value for the absolute integral of the white noise (Eq. 1) and S is the aforementioned signal intensity.

$$F(S,\sigma) = \frac{1}{\sqrt{2\pi}\sigma}\int_{-\infty}^{+\infty}|x|exp\left(-\frac{(x-S)^2}{2\sigma^2}\right)dx = \sqrt{\frac{2}{\pi}}\sigma\cdot exp\left(-\frac{S^2}{2\sigma^2}\right) - S\cdot erf\left(-\frac{S}{\sqrt{2}\sigma}\right) \quad \text{(S2)}$$

Analysis considering the micelle size distribution

Using the original optimized parameters, **Fig. 10a1** showed a right-shifted optimal build-up time and an overestimated optimal contrast factor, which can mostly be accounted for by the fact that the sizes of the target and background in the model are averaged values of the distribution of sizes of reverse micelles and their distance in actual samples. Concerning the size of the reverse micelles, the smaller ones influence the shape of the build-up of the contrast factor more strongly than the larger ones. **Fig. S5** shows the simulated build-up of the contrast factor with a distribution of x_T. Each panel has the same mean value of $\bar{x}_T = 6.43\ nm$ but a gradually broader distribution. Panel (a) shows the average results of five simulations, each with $x_T = 4.43, 5.43, \ldots 8.43\ nm$, panel (b) shows the average results of nine simulations, each with $x_T = 2.43, 3.43, \ldots 10.43\ nm$, and panel (c) shows the average results of thirteen simulations, each with $x_T = 0.43, 1.43, \ldots 12.43\ nm$. The optimal build-up time is clearly left-shifted, and the values of the contrast factor are lowered by the broader distribution of x_T, similar to the experimental results in **Fig. 7**. Note, however, that the exact distribution of parameters can be underdetermined when extracted from the experimental data by fitting and optimization.

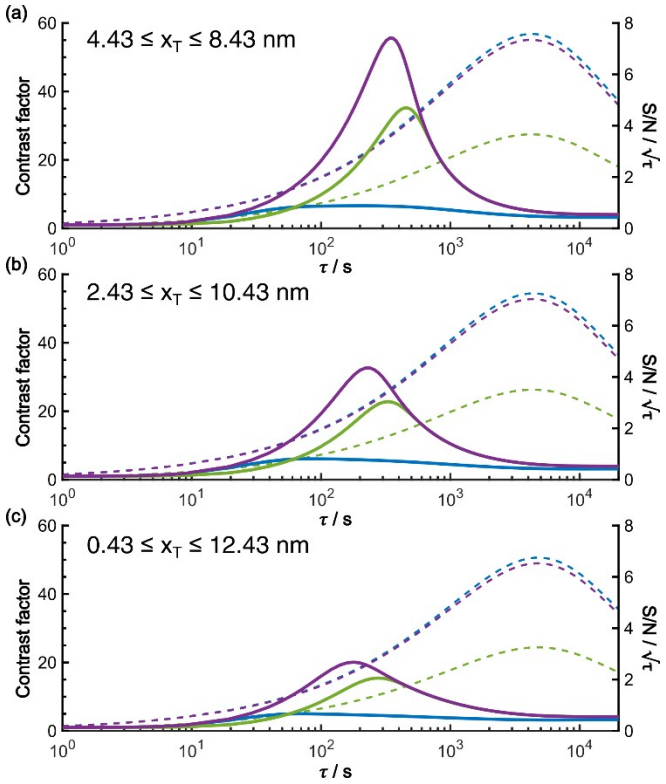

Fig. S5 Simulated build-up of the contrast factor with a distribution of x_T. The distributions of x_T are given in each panel. Other conditions of the simulation and the color order of plotting are the same as in Fig. 10a1.

1 W. R. Gambill, *Chem. Eng.*, 1959, **66**, 151–152.

2 D. B. Alger, *J. Chem. Educ.*, 1991, **68**, 939.

3 A. A. Bobko, I. Dhimitruka, J. L. Zweier and V. V. Khramtsov, *J. Am. Chem. Soc.*, 2007, **129**, 7240–7241.

4 S. N. Trukhan, V. F. Yudanov, V. M. Tormyshev, O. Yu. Rogozhnikova, D. V. Trukhin, M. K. Bowman, M. D. Krzyaniak, H. Chen and O. N. Martyanov, *J. Magn. Reson.*, 2013, **233**, 29–36.